THE JOURNAL OF PHYSICAL CHEMISTRY B

Article

pubs.acs.org/JPCB

Dual Fluorescence of Fast Blue RR and Fast Violet B: Effects of Solvents and Cyclodextrin Complexation

A. Antony Muthu Prabhu, R. K. Sankaranarayanan, G. Venkatesh, and N. Rajendiran*

Department of Chemistry, Annamalai University, Annamalai Nagar, 608 002 Tamilnadu, India

ABSTRACT: Absorption and steady-state and time-resolved fluorescence spectra of fast blue RR (FBRR) and fast violet B (FVB) were studied in solvents with different polarities and in the presence of α- and β-cyclodextrins (CDs). Dual emission observed in nonpolar solvents suggested that the energy of the intramolecular charge transfer (ICT) state is lower than that of the locally excited state. The normal Stokes-shifted band originated from the locally excited state, and the large Stokes-shifted band was due to the emission from a planar intramolecular charge transfer (PICT) state. The ratio of the PICT emission to the normal emission increased with β-CD concentration, whereas it was constant upon addition of α-CD. This behavior is in accordance with CD-dependent decay times of PICT and normal emissions, indicating the formation of different 1:1 FBRR/CD inclusion complexes. The rise time for the PICT emission increased with β-CD concentration, whereas no rise time was observed in the case of the α-CD complex. The size of the dimethoxyaniline ring suggested that the orientation of FBRR in the β-CD complex was different from that in the α-CD complex. The benzamido moiety of FBRR is deeply encapsulated in the CD cavity, whereas the aniline ring is exposed to the hydrophilic part. Semiempirical quantum-mechanical (ΔE, ΔG, ΔH, ΔS, and HOMO−LUMO) calculations were also carried out to assign the encapsulation of FBRR and FVB.

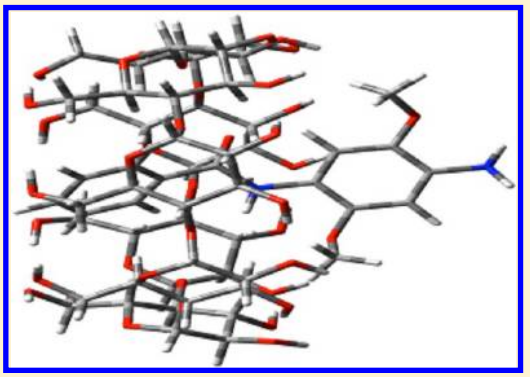

1. INTRODUCTION

Ever since the work of Lippert et al.,[1] the dual fluorescence of (*N*,*N*-dimethylamino)benzonitrile (DMABN) has been studied extensively and reviewed,[2,3] because its long-wavelength emission maxima, band widths, and molecular mobility changes are very sensitive to the solvation and polarity of the solvents. These properties make this molecule a very good reporter of its microenvironments; for example, DMABN has been used effectively in structural investigations of aqueous micelles,[4,5] cyclodextrins,[6,7] and polymers.[8,9]

A number of mechanisms have been proposed to explain this dual fluorescence,[2] but the mechanism proposed by Grabowski et al.[10] stands out and is known as twisted intramolecular charge transfer (TICT). The TICT mechanism involves the tortional motion of a dimethylamino group in conjugation with electron transfer along the pathway of the adiabatic photoreaction channel. The formation of TICT depends on two factors: (i) steric hindrance to planarity and (ii) an increase of the donor−acceptor character. In general, the electron-donor groups are amino or *N*,*N*-dimethylamino groups, and the electron-acceptor groups are —C≡N, —COOH, —COOR, etc. Other kinds of molecules have also been synthesized that have exhibited TICT emission, as detailed in the review article by Rettig.[2]

Further, a variety of alternative models have also been proposed to explain the dual emission of DMABN.[11a] There was generally a valid experimental reason for the introduction of the alternative reaction mechanisms. The proton-transfer model advocated by Kosower and Dodiuk,[11b] for example, was based on the interesting observation that the charge transfer (CT)/locally excited (LE) fluorescence intensity ratio for DMABN is considerably larger in deuterated ethanol (C_2H_5OD) than in normal ethanol. Similarly, the model based on specific solute−solvent interactions proposed by Visser and Varma[11c] originated from experiments showing that small amounts of polar solvents added to solutions of DMABN in nonpolar solvents far outweighed the bulk properties of the medium such as the polarity.

Whereas Lippert et al.'s model was concerned with the nature and molecular properties of excited-state levels, the TICT hypothesis is defined in terms of the molecular structure of the final equilibrated CT state. Other mechanisms, such as that of Zachariasse et al.,[12−14] which considers the planar intramolecular charge transfer (PICT) model[13,14] in which the CT state is planar, likewise make a statement on the molecular structure of the final CT state and do not directly identify the detailed pathway or the reaction dynamics of the ICT reaction from the ground state S_0 through the locally excited (LE) state to the equilibrated CT state.

Moreover, Zachariasse et al.[13,14] presented the evidence for dual fluorescence and ICT appearing in DMABN molecules: (i) a relatively small energy gap $\Delta E(S_1,S_2)$ between the two lowest excited singlet states and (ii) an energy barrier for the change in configuration of the amino group from pyramidal

Received: March 6, 2012
Revised: June 9, 2012
Published: June 15, 2012

dx.doi.org/10.1021/jp302162g | *J. Phys. Chem. B* 2012, 116, 9061−9074

toward planar that is small enough to allow the ICT reaction to occur within the fluorescence lifetime of the locally excited (LE) state of the aminobenzonitrile. It has been suggested that vibronic coupling between S_1 and S_2 is an essential element in the ICT reaction.[12−14] Such a coupling clearly depends on the magnitude of $\Delta E(S_1,S_2)$. Further, the change in the molecular configuration of the amino group is an important reaction coordinate in the ICT process of dual-fluorescent 4-aminobenzonitriles. With electron-donor-/acceptor-substituted naphthalenes, ICT has been observed when the energy gap $\Delta E(S_1,S_2)$ is sufficiently small for vibronic coupling to take place, such as with 1-dimethylamino-4-cyanonaphthalene.[13]

Recently, we studied many molecules in which the proton-donor groups were —NH_2, —OCH_3, and —OH, and the proton-acceptor groups were N═N, ═N—, C═O, etc. In our earlier studies, fast violet B,[15] 2-amino-3-benzyloxypyridine,[16] sulfanilamides,[17] hydroxybenzaldehydes,[18] aminobenzoic acids,[19] and azo[20] molecules were investigated. In the present work, the electron-acceptor group is the benzamido moiety, and the donor group is the aniline ring. Because the CO group is a better electron acceptor than −SO_2NH—, it might facilitate the formation of the ICT state more in fast blue RR and FVB (Figure 1) than in sulfanilamides and hydroxybenzaldehyde. The main aims of the present study were (i) to compare the effects of the electron-withdrawing fast blue RR (FBRR, 4-amino-2,5-dimethoxybenzanilide or 4-benzoylamino-2,5-dimethoxyaniline) and fast violet B (FVB, 4-amino-5-methoxy-2-methylbenzanilide) molecules on the ICT emission, (ii) to determine whether the inclusion complexes increase or decrease the long-wavelength (LW) emission, and (iii) to find adequate molecular probes. The results were obtained by UV−visible, steady-state fluorescence, time-resolved fluorescence, and ^{1}H NMR measurements and molecular modeling.

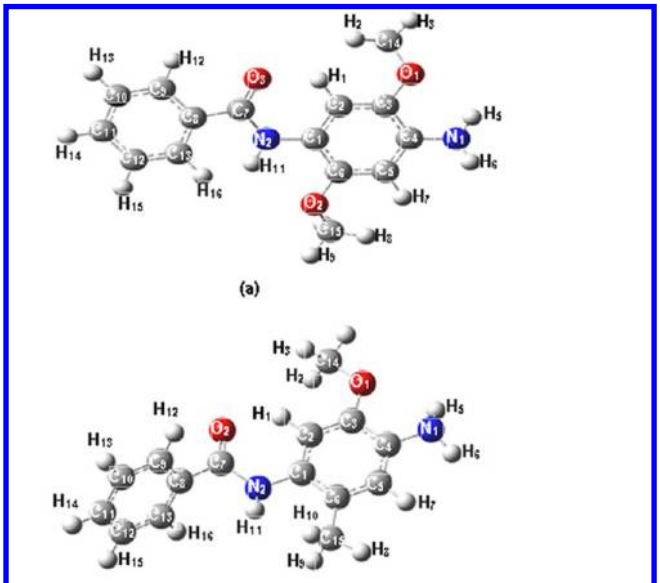

Figure 1. Optimized structures of (a) FBRR and (b) FVB.

2. MATERIALS AND METHODS

2.1. Reagents and Materials. FBRR, FVB, α-CD, β-CD, and spectro-grade solvents were purchased from Aldrich and used without further purification. All solvents were checked for spurious fluorescence in the region of the fluorescence measurements. The purity of the compounds was checked by similar fluorescence spectra when excited at different wavelengths. Analytical-grade sulfuric acid, *ortho*-phosphoric acid, and sodium hydroxide (E Merck) were used as received. Triply distilled water was used for the preparation of aqueous solutions. Aqueous solutions with pH values below 2.0 and above 11.5 were prepared by adding appropriate amounts of dilute (~10^{-3} M) solutions of NaOH and H_3PO_4. All spectral measurements were performed at a solute concentration of 2×10^{-5} M. The concentrations of α-CD and β-CD in solution were varied from 1×10^{-3} to 10×10^{-3} M. The quantum yields were determined[21] for solutions having absorbance values of less than 0.5 at the excitation wavelength using quinine sulfate in 0.1 N H_2SO_4 as the standard ($\varphi_f = 0.55$). The error limits for the fluorescence quantum yield and lifetime were 10% and 2−4%, respectively.

2.2. Synthesis of Inclusion Complexes. A methanol solution of FBRR or FVB (1 m mol, 10 mL) was added dropwise to an aqueous solution of CD (1 mmol, 40 mL), and the reaction mixture was stirred at 50 °C for 6 h. After the mixture had been cooled to room temperature, the precipitate (white powder) was collected by filtration. The crude product was dissolved in hot water to make a saturated solution. After removal of the insoluble substances by filtration, a small amount of water was added to the filtrate. The resultant solution was kept at room temperature for several days, and the white powder was collected for ^{1}H NMR analysis.

2.3. Instruments. Absorption spectral measurements were carried out with a Shimadzu UV 1601 PC model UV−visible spectrophotometer, and steady-state fluorescence measurements were made using a Shimadzu model RF-5301 spectrofluorimeter. The pH values of the solutions were measured in a Elico model LI-120 pH meter. A Bruker Advance DRX 400 MHz superconducting NMR spectrophotometer (IISc, Bangalore, India) was used to obtain ^{1}H NMR spectra. The fluorescence lifetime measurements were performed using a picosecond laser and a single-photon-counting setup from Jobin-Yvon IBH (Madras University, Chennai, India). A diode-pumped Millena CW laser (Spectra Analysis) at 532 nm was used to pump the Ti-sapphire rod in a Tsunami picosecond mode-locked laser system (Spectra Physics, model 4690 M3S). The Ti-sapphire rod was oriented at the Brewster's angle to the laser beam. The wavelength turning range was 280−540 nm (i.e., standard pico configuration). The fluorescence decay of the sample was analyzed using IBH data analysis software. The fluorescence decay profiles were fitted to the expressions

dx.doi.org/10.1021/jp302162g | J. Phys. Chem. B 2012, 116, 9061−9074

Table 1. Absorption and Fluorescence Spectral Data (nm), Quantum Yields, Lifetimes (ns), and Stokes Shifts (cm^{-1}) of FBRR and FVB in Selected Solvents and CD[a,b]

		FBRR[c]						FVB[d]					
no.	solvent	λ_{abs}	log ε	λ_{flu}	φ_f	τ	Stokes shift	λ_{abs}	log ε	λ_{flu}	φ_f	τ	Stokes shift
1	cyclohexane	327	sat	345	0.47	–	1595	306	sat	325	0.44	–	1910
		213		370 (sh)	0.22		3554	240 (sh)		360	0.22		4901
2	1,4-dioxane	328	4.16	347	0.51	0.38	1669	298	4.22	336	0.49	0.32	3795
		242	4.15	428	0.22	0.20	7123	240 (sh)	4.12	428	0.22	0.27	10192
3	ethyl acetate	328	4.08	344	0.53	0.41	1418	298	3.95	335	0.50	0.35	3706
		245	3.97	448	0.22	0.34	8166	240 (sh)	4.15	450	0.23	0.32	11334
4	acetonitrile	325	3.91	343	0.58	0.44	1614	300	3.89	345	0.54	0.34	4347
		246	3.89	449	0.25	0.29	8497	240 (sh)	4.11	450	0.24	0.30	11111
5	*t*-butyl alcohol	326	3.98	346	0.57	0.39	1773	298	3.91	345	0.57	0.30	4571
		246	3.65	454	0.19	0.30	8648	240 (sh)	4.09	455	0.21	0.27	11579
6	2-butanol	325	4.20	345	0.42	0.35	1783	298	3.89	345	0.41	0.28	4571
		246	3.85	453	0.18	0.28	8694	240 (sh)	4.14	455	0.19	0.26	11579
7	2-propanol	327	4.02	345	0.41	0.36	1595	295	3.93	348	0.36	0.29	5162
		240	4.35	455	0.18	0.28	8603	240 (sh)	4.15	455	0.14	0.25	11920
8	methanol	318	3.98	345	0.35	0.34	2461	294	3.92	346	0.31	0.29	5111
		238	4.37	454	0.13	0.26	9420	240 (sh)	4.14	455	0.12	0.25	12035
9	water (pH 6.5)	304	3.49	348	0.17	0.26	4159	291	3.73	350	0.15	0.25	5792
		235	4.42	454	0.10	0.25	10868	240 (sh)	4.10	455 (w)	0.07	0.23	12386
10	0.01 M α-CD	304	4.06	350	0.18	0.27	4323	270	4.20	349	0.18	0.26	8384
		234	4.66	455 (w)	0.27	0.28	10916	220	4.61	455	0.15	0.27	15051
	0.01 M β-CD	304	4.06	350	0.19	0.29	4323	270	4.20	337	0.20	0.30	8384
		234	4.66	455	0.73	0.34	10916	240	4.61	454	0.68	0.42	15051

[a]sat, saturated; sh, shoulder; w, weak. [b]Error limits: φ_f, 10%; τ, 2–4%. [c]Onsager cavity radius (Å) = 6.45. Correlation coefficient for $E_T(30)$ versus $\Delta\bar{\nu}$ = 0.7444. Correlation coefficient for Δf versus $\Delta\bar{\nu}$ = 0.1913. ΔG (kcal mol^{-1}) = abs: −15.84 and flu: −20.00. [d]Onsager cavity radius (Å) = 6.12. Correlation coefficient for $E_T(30)$ versus $\Delta\bar{\nu}$ = 0.7015. Correlation coefficient for Δf versus $\Delta\bar{\nu}$ = 0.6751. ΔG (kcal mol^{-1}) = abs: −15.24 and flu: −19.80.

$$I(t) = A_1 \exp\left(\frac{-t}{\tau_1}\right) + A_2 \exp\left(\frac{-t}{\tau_2}\right) \quad (1)$$

$$I(t) = A_1 \exp\left(\frac{-t}{\tau_1}\right) + A_2 \exp\left(\frac{-t}{\tau_2}\right) + A_3 \exp\left(\frac{-t}{\tau_3}\right) \quad (2)$$

where τ_1, τ_2, and τ_3 are lifetimes of the three components; a_1 a_2, and a_3 are the corresponding pre-exponential factors, and t is the time. The average fluorescence lifetime was calculated using the equation

$$\langle\tau\rangle = \sum \tau_i a_i \quad (3)$$

2.4. Molecular Modeling Studies. The theoretical calculations were performed using Gaussian 03W. The calculations were carried out in the gas phase, so solvent effects were not taken into account in the calculations. The initial geometries of the guest and CD molecules were constructed with Spartan 08 and then optimized by the PM3 method. α- and β-CD were fully optimized by PM3 without any symmetry constraints.[22] Because the semiempirical PM3 method has been shown to be a powerful tool in the conformational study of cyclodextrin complexes and has high computational efficiency in calculating CD systems,[22] it was selected to study the inclusion process of CD with FBRR and FVB in this work.

3. RESULTS AND DISCUSSION

3.1. Effect of Solvents. *3.1.1. Absorption Spectrum.* The absorption and fluorescence spectra of FBRR and FVB were recorded in different solvents, and the band maxima, log ε_{max} values, quantum yields (q_{fl}), excited-state lifetimes, and Stokes shifts are compiled in Table 1. Because of the very low solubilities of FBRR and FVB in cyclohexane, the absorption maxima were obtained using 1% diethyl ether solutions of cyclohexane. The absorption maxima should be very near those obtained in pure cyclohexane because the polarity of diethyl ether is close to that of cyclohexane. Further, the trend observed in the absorption maxima of FBRR and FVB in cyclohexane was similar to that observed in other solvents. As for other aromatic amines[15−19] and similar analogues of benzanilide,[15] the LW absorption band maximum was blue-shifted with increased polarity and hydrogen-bond-forming capacity of the solvents. Also, the absorption spectra of FBRR and FVB were red-shifted in comparison to that of their unsubstituted amino derivative (i.e., benzanilide, BA).[15b] When compared to FVB, the red shift observed in the LW absorption band of FBRR is due to the presence of two methoxy groups at the aniline moiety. The red shifts observed in the LW band that are larger than for their amino compounds also depend on other substituents.

The absorption spectral characteristics of FBRR are very similar to those of its analogue (BA),[15] namely, very large molecular extinction coefficients (Table 1). The results suggest that the LW absorption band can be assigned to the π–π^* transition. Further, the results observed for FBRR are also similar to those observed for FVB. Thus, it can be suggested that the LW transitions in FBRR and FVB originating from the aniline ring and benzamido moiety might be perturbing this transition.

3.1.2. Fluorescence Spectrum. The fluorescence spectra of FBRR and FVB exhibited dual fluorescence in all of the

dx.doi.org/10.1021/jp302162g | J. Phys. Chem. B 2012, 116, 9061−9074

solvents investigated (Figure 2). Considering DMABN as a reference molecule, the short-wavelength (SW) or locally

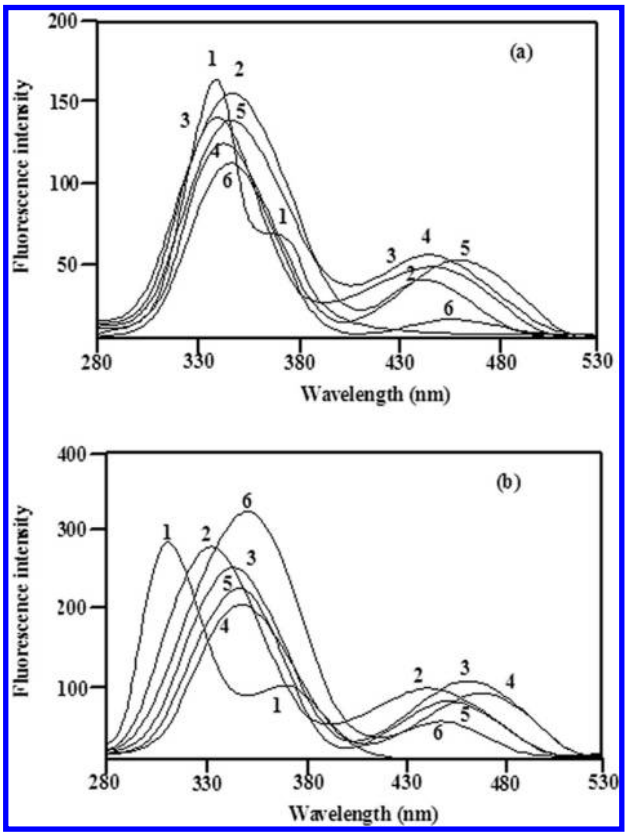

Figure 2. Fluorescence spectra of FBRR and FVB in selected solvents (concentration $\approx 4 \times 10^{-5}$ M): (1) cyclohexane, (2) ethyl acetate, (3) acetonitrile, (4) *t*-butyl alcohol, (5) methanol, and (6) water.

excited (LE) band and the long-wavelength (LW) or ICT band are defined as the B band and the A band, respectively. The fluorescence quantum yields (φ_f) obtained for FBRR and FVB in all of the solvents excited at 310 nm were calculated using the absorbance at that wavelength. The fluorescence band maxima and quantum yields of FBRR were found to be nearly equal to those of FVB. The φ_f values decreased slightly with increasing polarity of the solvents. The decrease in φ_f for both wavelength emissions in going from aprotic solvents to water was quite large.

The area under the A band decreased with the increase in the polarity and hydrogen-bonding capacity of the solvents and was nearly absent in water. The fluorescence band maxima of both bands were red-shifted in going from nonpolar to polar solvents, and the red shift of the A band was greater than that of the B band. The ratio of the fluorescence intensity of the A band to that of the B band in FBRR and FVB at their respective maxima decreased with increasing polarity of the solvents. The solvatochromic effects on the B band were studied using a Lippert–Mataga plot[23] (eq 4) and the $E_T(30)$ parameter[24,25]

$$\Delta\bar{\nu}_{ss} = \frac{2(\mu_e - \mu_g)^2}{hca^2} f(D, n) + c \tag{4}$$

where $\Delta\bar{\nu}_{ss}$ is the Stokes shift ($\Delta\bar{\nu}_{ss} = \bar{\nu}_{abs,max} - \bar{\nu}_{flu,max}$); μ_g and μ_e are the ground-state and excited-state dipole moments, respectively; h is Planck's constant; c is the velocity of light; a is the Onsager cavity radius; and Δf is defined as

$$f(D, n) = \frac{D - 1}{2D + 1} - \frac{n^2 - 1}{2n^2 + 1} \tag{5}$$

where ε is the dielectric constant and n is the refractive index. Although the Lippert–Mataga plot does not take into account the polarizability effects and the deviation from colinearity of μ_g and μ_e, it is simple and explains nicely the results observed in polar/aprotic solvents. According to Lippert et al.'s method,[23] the value of a was taken as ~50% of the long axis of the molecule (obtained from the optimized structures of FBRR and FVB obtained using the PM3 method), or 6.45 and 6.12 Å for FBRR and FVB, respectively. Figure 3 depicts a plot of the

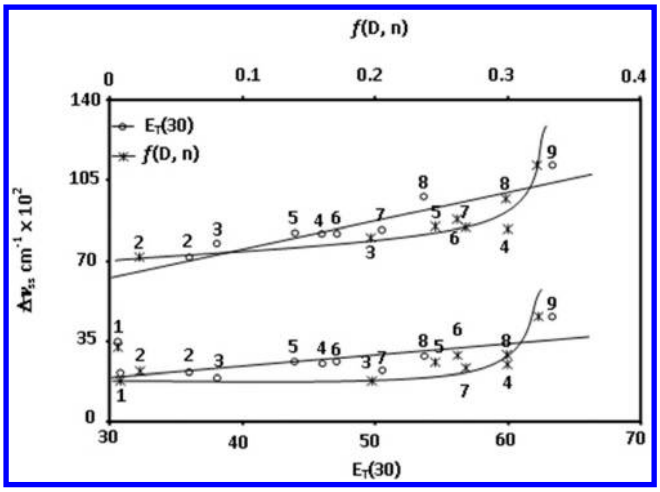

Figure 3. Plot of Stokes shifts (cm^{-1}) of FBRR versus $E_T(30)$ and $f(D,n)$ solvent parameters: (1) cyclohexane, (2) dioxane, (3) ethylacetate, (4) acetonitrile, (5) *t*-butyl alcohol, (6) 2-butanol, (7) 2-propanol, (8) methanol, and (9) water.

Stokes shift versus Δf or $E_T(30)$ for the A and B bands. Because the Lippert–Mataga plot does not take into account the specific interactions of protic solvents, such as hydrogen bonding, the Δf plot was nonlinear in protic solvents, as expected. Because the $E_T(30)$ parameters do take into account the specific interactions (hydrogen bonding) in addition to the dispersive interactions, the plot between the Stokes shift and $E_T(30)$ was linear (Figure 3). The slope of the linear part of the plot of the Stokes shift versus $E_T(30)$ gave the polarity parameter (Figure 3) for the B band as 3132 cm^{-1}. Taking dipole moments (μ_g) of ~2.81 and 3.11 D for FBRR and FVB, respectively, as obtained by the PM3 method, the values of μ_e obtained for the B* state were found to be 9.02 and 9.64 D, respectively. The Lippert–Mataga plot could not be used to study the solvatochromic effects on the A band because the absorption spectrum corresponding to the A species is not available. Thus, the fluorescence data for the A band were evaluated from the following equation, originally derived by Beens et al.[26] for the exciplex emission

$$E_A = (E_A)_0 - [2\mu_e^2(A)/hca^3]\Delta f \tag{6}$$

where Δf is defined as

$$\Delta f = [(\varepsilon - 1)/(2\varepsilon+1)] - \left[\frac{1}{2}(n^2 - 1)/(2n^2 + 1)\right] \tag{7}$$

E_A and $(E_A)_0$ are the energies of the A band in a given solvent and in air, respectively, and the other terms have the same meanings as provided earlier. The plots of E_A (cm^{-1}) and Δf

dx.doi.org/10.1021/jp302162g | J. Phys. Chem. B 2012, 116, 9061–9074

(kcal mol^{-1}) versus $E_T(30)$ (Figure 3) were found to be linear. The values of μ_e (A) calculated from the linear part of the former plot were found to be 13.2 and 14.71 D for FBRR and FVB, respectively. In other words, as expected, the dipole moment of the A* state was higher than that of the B* state.

The effect of excitation wavelength (λ_{exc}) in the range of 300−360 nm was studied in acetonitrile. It was observed that the fluorescence maxima of both bands and the fluorescence quantum yields were independent of λ_{exc}. This indicates that the emissions from both states are occurring from their most relaxed states and that the solvent relaxation times of these solvents are smaller than the radiative decay rate of the fluorophore. The fluorescence excitation spectra (Figure 4)

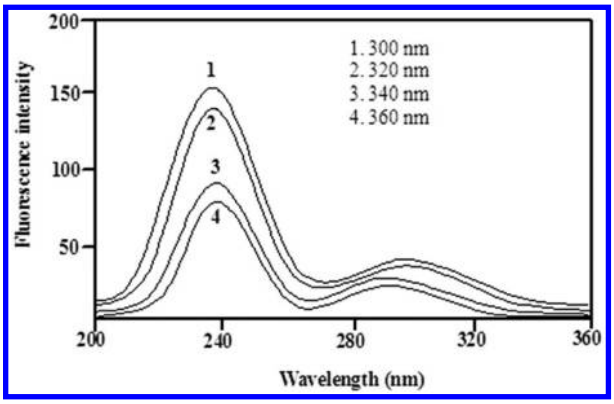

Figure 4. Fluorescence excitation spectra of FBRR measured in acetonitrile at different emission wavelengths.

recorded in acetonitrile (emission wavelength 300−360 nm) resembled each other, as well as, the absorption spectra. This indicates that the absorbing species in the ground state for both emissions were the same.

Although several mechanisms have been proposed to explain the A-band emission, the mechanism proposed by Grabowski et al.[10] and Zachariasse et al.[12−14] is still considered to be the best. Our results can also be explained along the same lines by rejecting the other mechanisms: A-band emission originating from impurities can be rejected on the grounds that both emissions are insensitive to λ_{exc} and no changes were observed during the experiment in the spectral features or in the fluorescence spectra of FBRR and FVB measured on freshly prepared solutions or when different excitation wavelengths were used. It was observed that (1) the ratios of the fluorescence intensities at the respective maxima of A and B did not change over the concentration range of 10^{-5}−10^{-4} M and (2) a vibrational structure appeared in the nonpolar solvents. Thus, A-band emission arising from excimer formation[27−29] can be rejected.

Because many examples in which A-band emission has been observed in nonpolar solvents are now available in the literature,[1] the initial proposal of solvent-assisted level reversal of S_2 and S_1 by Lippert et al.[1] can be rejected. Further, the fluorescence excitation spectra recorded at the two emissions are similar to the absorption spectrum, so it can be concluded that both the A and B emissions originate from the two different excited states. Large Stokes shifts have been observed in molecules showing ICT behavior: for example, 9420 cm^{-1} for FBRR and 12035 cm^{-1} for FVB in methanol. Almost similar Stokes shifts were also observed for the present molecules in cyclohexane: 3554 and 4901 cm^{-1} for FBRR and FVB, respectively. Because proton transfer is highly improbable in hydrocarbon solvents, an excited-state proton-transfer mechanism as proposed by Kosower and Dodiuk[29] for DMABN can also be rejected.

The fluorescence intensity increased when the concentration of aprotic/nonpolar solvents in water increased; that is, the fluorescence spectrum in water solution changed significantly upon addition of water/dioxane, showing a dual emission (Figure 5). It is noted that, in contrast to the behavior of other

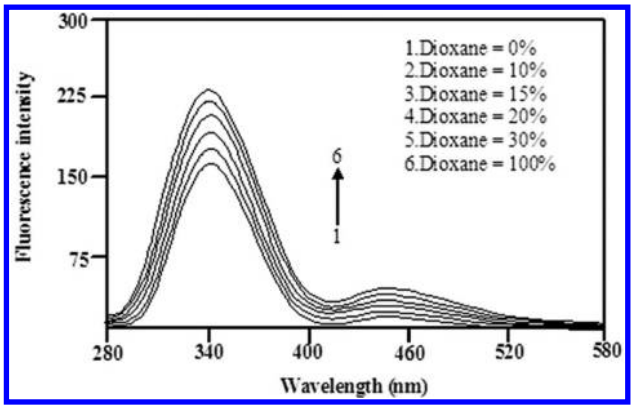

Figure 5. Fluorescence emission spectra of FBRR in water−dioxane mixed solvents (excitation wavelength = 265 nm).

polar solvents, the intensity of emission in water further decreased even though the normal emission intensity is nearly independent of the hydrogen-bonding ability of the solvents. These observations suggest that the dual emission of FBRR and FVB in water/acetonitrile seems to be influenced by the enhanced intermolecular hydrogen bonding of the carbonyl group in the excited state.[30] Supporting this hypothesis, the fluorescence spectrum in aqueous solution changed significantly upon addition of acetonitrile, showing dual emission in acetonitrile−water mixture (Figure 6).

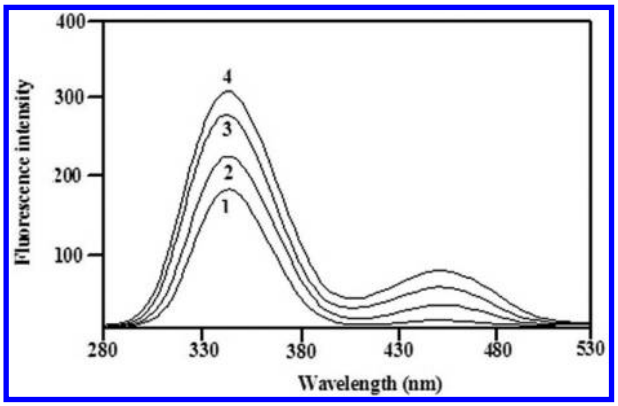

Figure 6. Fluorescence spectra of FBRR in water with acetonitrile: (1) water, (2) water with 5% acetonitrile, (3) water with 10% acetonitrile, and (4) water with 10% acetonitrile.

The spectral resemblance of FBRR and FVB suggests that the results can also be explained along similar lines; that is, the small Stokes-shifted band can be assigned to the locally excited state (B band), and the large Stokes-shifted band can be assigned to the ICT state. Two types of rotational motions in FBRR are possible for the origination of the ICT band: (a) rotation of the —NH_2 group around the C—N bond and (b)

dx.doi.org/10.1021/jp302162g | J. Phys. Chem. B 2012, 116, 9061−9074

Table 2. Geometrical Parameters of FBRR and FVB before and after Inclusion in α-CD and β-CD for the Most Stable Inclusion Complexes

property	FBRR		FBRR:α-CD	FBRR:β-CD	FVB	FVB:α-CD	FVB:β-CD
bond length (Å)	H14—H5	12.24	12.29	12.16	12.20	12.09	12.21
	H14—N2	6.16	6.19	6.13	6.12	6.11	6.15
	H4—H9	9.14	9.15	8.97	7.89	7.93	7.87
hydrogen bond length (Å)	(>C═O)O3···H(2°OH)		3.69	4.34		3.24	4.57
	(—NH)H11···O(2°OH)		4.44	5.27		4.25	4.08
	(—OCH_3)O2···H(2°OH)			3.92			
bond angle (deg)	C8—C7—O3	122	122	123	123	123	123
	O3—C7—N2	120	120	119	121	120	120
	C7—N2—H11	113	114	114	114	113	113
	C1—N2—H11	114	114	114	113	113	113
dihedral angle (deg)	C8—C7—O3—N2	−175	174	−178	−175	−177	−177
	O3—C7—N2—H11	166	−166	168	166	168	164
	C1—N2—H11—C7	149	−149	149	149	145	149

rotation of the complete aniline moiety around the C—N bond. Earlier studies on 2-(4′- aminophenyl)benzazoles[31,32] showed that these molecules exhibit only a single normal Stokes-shifted fluorescence band from the locally excited states, and the vibrational structure of the B band matches that of 2-phenyl-substituted benzazoles. Moreover, if rotation had occurred around the C—NH_2 bond, a blue shift in the position of the B band relative to that of the respective 2-phenyl derivative should have been observed. Thus, it would not be unreasonable to mention that the rotation of the aniline ring around the C—N bond is responsible for the ICT emission and not the rotation of the complete benzamido moiety. Further, it is now well-known that the energy barrier for the formation of A from B decreases as the polarity of the medium increases,[33,34] that is, the emission intensity of A should increase in going from nonpolar to polar solvents. The opposite results observed in the present molecule can be explained in the following manner: As seen above, the dipole moment of the ICT state is very large, and the dipolar interactions of the ICT state will increase with increasing polarity of the solvent. Thus, the decrease in the fluorescence intensity of the A band in polar solvents could be due to large stabilization of the highly polar ICT state by strong dipole−dipole and hydrogen-bonding interactions and consequent rapid nonradiative transition to the ground and/or low-lying triplet states.[35]

To obtain a better understanding of the structures of FBRR and FVB, molecular modeling geometry optimizations were carried out by the PM3 method. The optimized structures showed both the benzamido and aniline rings present in planar positions (Figure 1). The bond angles and dihedral angles were also not twisted as in other TICT molecules (Table 2). The enhancement of the normal emission bands of FBRR and FVB in nonpolar and aprotic solvents might be due to lowering of the solvent polarity and raising of the energy of the ICT state, causing an increase in the energy barrier for transition between the LE and ICT states. As mentioned in the Introduction, the above results predict that the dual emission is caused by the presence of PICT in both molecules.

Zachariasse et al.[12−14] pointed out inadequacies in the TICT model and molecules that are constrained to remain planar but show ICT emissions, which they described as planar intramolecular charge transfer (PICT) emissions. They discussed molecules (3DMABN) that were identical with regard to Grabowski et al.'s[10] and Rettig's[2] predictions [using simple estimations of the energetics of charge transfer (CT) from the donor to the acceptor part of the molecule] of ICT characteristics to the TICT molecules (4DMABN) but that did not show dual emissions. Lippert et al.[1b] already pointed out that the presence of a small energy gap, $\Delta E(S_1,S_2)$, is directly correlated with the appearance of dual fluorescence in 4-aminobenzonitriles. The similarity of the spectral characteristics of FBRR and FVB suggests that the results can also be explained along the same lines. In the PICT model, independent of the structure of the ICT state, a small energy gap, $\Delta E(S_1,S_2)$, between the two lowest excited singlet states is considered to be an important requirement for the occurrence of dual fluorescence.[14] In the PICT model, the S_2 (^1L_a, CT) state has a substantially larger dipole moment than the S_1 state (^1L_b), which preferentially decreases the energy relative of S_2 to that of S_1 (^1L_b) as the solvent polarity increases. When the energy gap, $\Delta E(S_1,S_2)$, is sufficiently small, a dynamic state reversal can occur after excitation, leading to an emitting ICT state alongside LE, and dual fluorescence appears. During the reaction from LE to ICT, changes in the molecular structure take place, involving the configuration of the amino nitrogen and the bond lengths in the molecule,[14] and these changes contribute to the magnitude of the ICT reaction barrier, E_a, and a destabilization energy, δE_{FC}, of the Franck−Condon (FC) ground state.

Having established that the two emissions originate from two different excited states having the same ground-state precursor, we tried to study their time-correlated behavior by measuring the lifetimes of the two emissions in different solvents. In each case, the fluorescence decay followed a single exponential, and the relevant data are compiled in Table 1. The lifetimes of both species increased slightly with increasing solvent polarity but decreased in polar/protic solvents. Further, the lifetimes of LE species are higher than PICT in aprotic solvents, but τ_A in CD is greater than τ_B.

The fluorescence decays of A (PICT) and B (LE) (Scheme 1) can be expressed as suggested by Kajimoto et al.,[36] where k_1 is the rate of formation of A*; k_2 is the rate of formation of B* from A*; and k_B and k_A are the sums of the radiative and nonradiative decay rates of B* and A*, respectively. It is well

Scheme 1

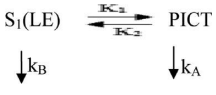

dx.doi.org/10.1021/jp302162g | J. Phys. Chem. B 2012, 116, 9061−9074

established that both A and B emissions follow double-exponential decay.[36,37] In the case of B*, the fast decay (on the order of nanoseconds) reflects the rate of charge transfer (k_1) from B* to A*, and the slow decay reflects the normal emission (k_2). On the other hand, the faster decay in A* reflects the rise time, and the slow decay reflects the normal emission of A* (k_1). The similar values of τ_A and τ_B in nonpolar and polar/aprotic solvents (Table 1) clearly suggest that equilibrium is established between B* and A* in a very short time. This is further supported by the fact that the lifetimes for the A* and B* states are not significantly different (i.e., 0.34 and 0.26 ns, respectively, in methanol).

3.2. Effect of Cyclodextrins. Figure 7 shows the absorption spectra of FBRR in aqueous buffer solutions (pH

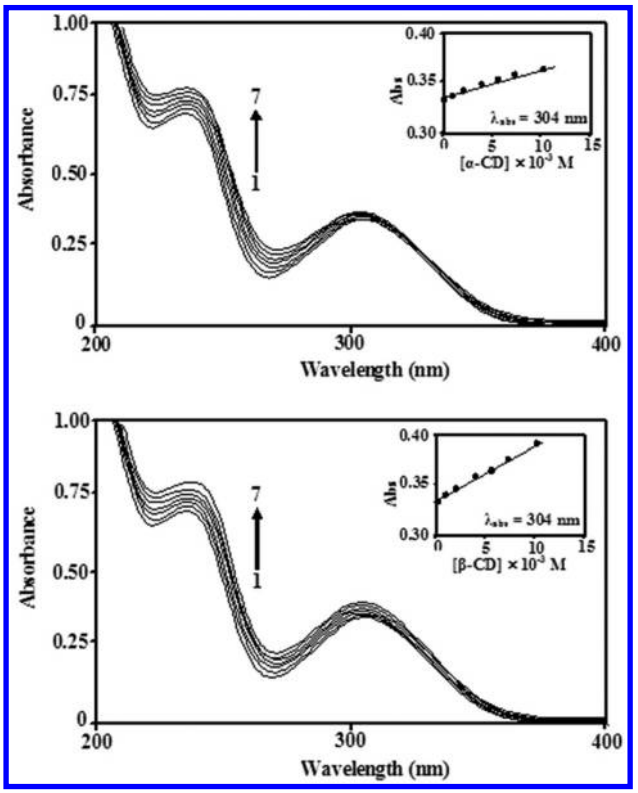

Figure 7. Absorption spectra of FBRR in different α- and β-CD concentrations (M): (1) 0, (2) 0.001, (3) 0.002, (4) 0.004, (5) 0.006, (6) 0.008, and (7) 0.01. Inset: absorbance versus α- and β-CD concentrations.

7.0) with different concentrations of α-CD and β-CD. Upon increasing the concentration of both CDs, the absorbance increased slightly at the same absorption maxima around 304 and 235 nm. The slight increase in the absorbance with the addition of CDs can be attributed to the enhanced dissolution of the guest molecule through the detergent action of CD,[38−40] indicating the formation of FBRR/CD complexes.

Figure 8 presents the fluorescence spectra of FBRR in aqueous solution as a function of α-CD or β-CD concentration, excited at 310 nm, where the CD dependent absorbance changes are negligible. In the CD-free aqueous solution, the typical dual fluorescence of PICT can be seen, even though the emission quantum yields of the normal emission around 350 nm and the PICT emission around 455 nm are extremely low. The weak PICT emission has been presumably ascribed to the stabilization of the highly polar PICT state by strong dipole−

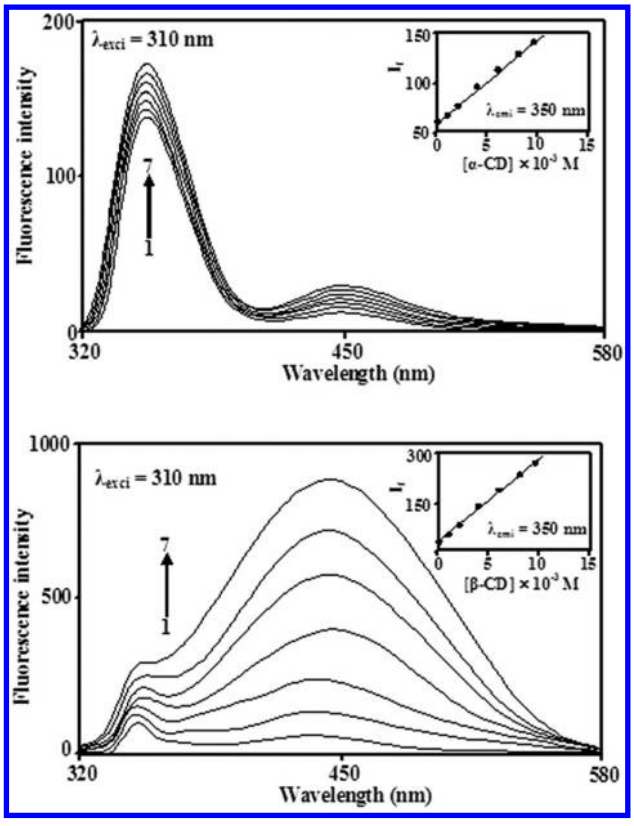

Figure 8. Fluorescence spectra of FBRR in different α- and β-CD concentrations (M): (1) 0, (2) 0.001, (3) 0.002, (4) 0.004, (5) 0.006, (6) 0.008, and (7) 0.01. Inset: Fluorescence intensity versus α- and β-CD concentrations.

dipole interactions with water and consequent rapid non-radiative transition to the ground and/or low-lying triplet state.[40] Upon addition of α-CD, both the normal and PICT emissions were slightly enhanced, whereas the emission maxima remained relatively unchanged (Figure 8 inset). The fluorescence intensity ratio of the PICT band and the normal band, I_a/I_b, were same when the concentration of α-CD increases. On the contrary, upon addition of β-CD to the aqueous solution of FBRR, the PICT emission band is rather strongly enhanced with little enhancement of the normal emission. In other words, as the concentration of α-CD increased, the I_a/I_b ratio decreased, in contrast to the increase observed in β-CD solution. It can be seen as further evidence for the formation of FBRR/CD inclusion complexes that the initial changes of the I_a/I_b ratios leveled off at high α-CD or β-CD concentration. It is also noteworthy that the PICT emission intensity effectively increased in β-CD; however, the changes in the normal emission upon addition of both CDs were very small. These opposite spectral changes in α-CD or β-CD solutions suggest that the structural geometry of the FBRR/α-CD inclusion complex is different from that of the FBRR/β-CD complex in terms of the orientations of the guest molecules.

To analyze the CD-induced changes in the fluorescence spectra of FBRR, we measured the emission decay of the normal (350 nm) and PICT (450 nm) emissions in aqueous buffer solutions (pH 7.0) containing different concentrations of α- and β-CD. Figure 9 shows the typical PICT emission decay profiles in the presence of α- and β-CDs. Analysis of these profiles and the normal emission decays is reported in Table 1.

dx.doi.org/10.1021/jp302162g | J. Phys. Chem. B 2012, 116, 9061−9074

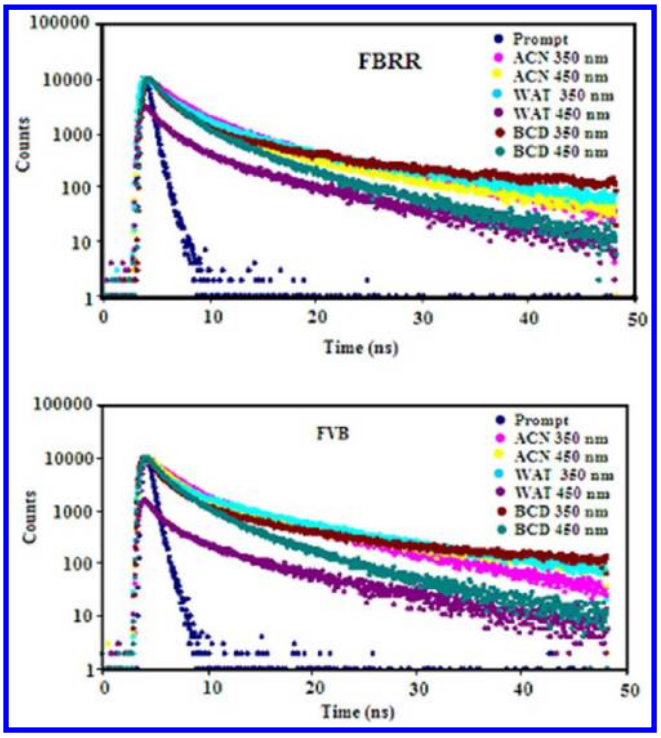

Figure 9. Fluorescence decay curves of FBRR and FVB in acetonitrile, water, and 0.01 M β-CD solution.

The normal emission decay in the absence of CD exhibits a slight fast decay (0.26 ns) as a major decay component with a small contribution of a slow decay component (0.25 ns). This decay behavior indicates the existence of two different normal emitting species that compete with the conformational relaxation times required for the PICT state. It is noteworthy that the decay time of the slow component was similar to that of PICT emission within experimental uncertainty. This indicates that equilibrium between the locally excited (LE) state and the PICT state was achieved in water in a rather short period. However, this was a coincidence in the presence of CD, revealing that the equilibrium between the LE and PICT states was modified by the formation of the CD inclusion complexes. The decay time of the fast component remained the same within experimental error even with increasing α-CD concentration, and its relative quantum yield increased significantly upon addition of α-CD, in contrast to its major change in β-CD solution. In the meantime, the decay time of the slow component increased significantly from water (0.26 ns) to 0.01 M α-CD and β-CD (0.28 and 0.29 ns, respectively). The relative quantum yield of the slow component increased upon addition of β-CD, whereas it was little changed upon addition of α-CD. This is consistent with the enhancement of the normal fluorescence in contrast to the minimal change in the presence of α-CD.

The decay time of the PICT emission was observed to be very short in aqueous solution and also influenced by the addition of β-CD. This behavior indicates the competing process between the conformational relaxation required for the PICT state and the fast decay process of the normal emission. Upon addition of α-CD, the PICT emission decay profile was weak triexponential decay without significant enhancement of the lifetime and the relative quantum yield. On the contrary, upon addition of β-CD, one decay component in the PICT emission (0.32 ns) appeared, suggesting the formation of different FBRR/α-CD and FBRR/β-CD inclusion complexes. The relative fluorescence quantum yields and their lifetimes did not change with the α-CD concentration. This is also consistent with the minimal enhancement of the PICT emission in the α-CD solution (Figure 9). The rise time of the PICT emission, which is different from the fast decay time of the normal emission, increased as the β-CD concentration increased, whereas it was not observed upon addition of α-CD. This reflects that the PICT dynamics of the FBRR/β-CD inclusion complex was quite different from that of the FBRR/α-CD complex.

To interpret the present results, we focus on three key observations of the PICT dynamics and steady-state emission properties, namely, (i) fast and slow relaxational processes are involved in the formation of the PICT state in water; (ii) the dynamics of the fast process is independent of the α-CD addition to water, whereas the rate of the slow process shows a linear dependence on the β-CD concentration and the fast process dominates in water; and (iii) the relative quantum yield of the fast process decreases significantly upon addition of β-CD, in contrast to the minimal change in the presence of α-CD.

The fast decay time (0.29 ns) of the normal emission corresponds to the rise of the PICT emission, and it is faster than the diffusion-controlled reaction time. Thus, we believe that the fast process is due to the excitation of the ground-state complex between FBRR/FVB and water through hydrogen bonding as observed for FBRR/FVB in water/dioxane mixed solvent.[39] On the other hand, considering that the lifetime of the slow process increases upon addition of β-CD to water, this slow process probably reflects the existence of excited FBRR/FVB molecules without water molecules in their neighborhood or the proper arrangement of water molecules for PICT to occur. This slow relaxational process is mainly due to a long-range polarization interaction to further stabilize the PICT state. It is to be mentioned that these two processes are differently affected by different CDs; the relative quantum yield of the fast process decreases significantly, whereas that of the slow process increases upon addition of β-CD, in contrast to the minimal change in the quantum yield in the presence of α-CD.

The CD-dependent triexponential decay times of the normal emission led us to conclude that both the forward and reverse PICT rates in aqueous solution underwent a change in the presence of CD. Thus, the above results confirmed the more favorable formation of the PICT state in β-CD solution than in α-CD solution. The CD dependences of the PICT dynamics can be interpreted on the basis of different solvent−solute interactions induced by forming different patterns of CD inclusion complexes.

Because the fast process is due to the excitation of the ground-state complex between FBRR/FVB and water through hydrogen bonding, the different CD dependences of the relative quantum yields of the fast and slow relaxational processes imply that the hydrogen-bonding interactions between FBRR/FVB and water molecules in the presence of α-CD are different from those in the presence of β-CD. In other words, both the amino group and carbonyl group can be hydrogen-bonded with water, but the orientations of those two groups can be different with regard to the water molecule, by forming different patterns of CD inclusion complexes depending on the kind of CD.

The differences in the patterns of the inclusion complexes can be explained in terms of differences in the internal

dx.doi.org/10.1021/jp302162g | J. Phys. Chem. B 2012, 116, 9061−9074

diameters of the α- and β-CD cavities, as well as the dimensions of FBRR and FVB. To determine the dimensions of FBRR and FVB, the geometries of the molecules in the ground state were optimized using the PM3 program. These calculations revealed that the diameters of the two methoxy groups are about 9.14 Å, which is larger than those of the α- and β-CD cavities (5.6 and 6.5 Å, respectively).[41,42] Therefore, the benzamido ring of FBRR/FVB is entrapped in the α-CD or β-CD cavity with the amino and methoxy group exposed to the bulk phase. This should be why the absorption and emission maxima of the neutral and monocation for FBRR and FVB had the same values in the presence of CD as in its absence. On the basis of the different orientations of FBRR and FVB in α- and β-CDs, it is clear that the increase in the relative quantum yield of the fast component of normal emission upon addition of β-CD is due to the inhibition of hydrogen bonding between the carbonyl group and water. As long as the carbonyl group is exposed to water, the magnitude of the contribution of the fast relaxational process to the PICT state stays the same as observed in the α-CD inclusion complex. Because of the presence of a methoxy/methyl group at the sixth position in FBRR/FVB, respectively, the aniline ring becomes larger in size relative to the α-CD or β-CD cavity. This factor might also be responsible for the formation of different types of inclusion complexes in CD solution, as demonstrated by the two decay components of PICT emission.

Naturally, the formation of two different types of inclusion complex between FBRR/FVB and CDs is possible. One has the benzamido ring captured in the CD cavity, and the other has the aniline ring captured. In α-CD, benzamido ring encapsulation is more favorable, on average, than aniline ring encapsulation because of the larger size of the aniline moiety (i.e., dimethoxy group does not fit well to the rim of α-CD). Because the diameter of the β-CD cavity is higher than that of the α-CD cavity, —CONH— locates in the less polar environment of the β-CD cavity. Supporting this, the PICT intensity of FBRR is little increased with α-CD concentration, whereas that of β-CD, which effectively increased.[37−40] Further, the presence of an isosbestic point seems to indicate the formation of a well-defined 1:1 complex. Also, we attempted to evaluate the stoichiometry and binding constant of the inclusion complexes by monitoring the I_a/I_b ratio and using the Benansi-Hildebrand equation.[43]

Figure 10 shows a straight line from a plot of $1/\Delta A$ or $1/(I - I_0)$ versus the reciprocal of CD concentration ([CD]), and a plot of $1/\Delta A$ or $I/I - I_0$) versus $[CD]^2$ gives an upward curve for the present systems, indicating a 1:1 stoichiometry in the inclusion complexes. From the slope and intercept, the formation constant was determined. From Table 1, one can see the binding constant for FBRR/β-CD is larger than that for the FBRR/α-CD complex, because the orientation of FBRR in the α-CD inclusion complex is different. The binding constants (K) in the ground state are 278, 542, 225, and 425 M^{-1}, and those in the excited state are 623, 2820, 654, and 2597 M^{-1} for the inclusion complexes, α-CD:FBRR, β-CD:FBRR, α-CD:FVB, and β-CD:FVB, respectively. These data indicate that the guest:β-CD inclusion complex is more stable than the others, which can be explained by β-CD having the optimal size for its internal cavity (6.5 Å) to encase the guest molecule.

The large binding constant implies that the benzamido ring is more deeply embedded in the β-CD cavity than in the α-CD cavity and that the rotation of the amino aryl group for PICT would be inhibited. The increase in the rise time of PICT

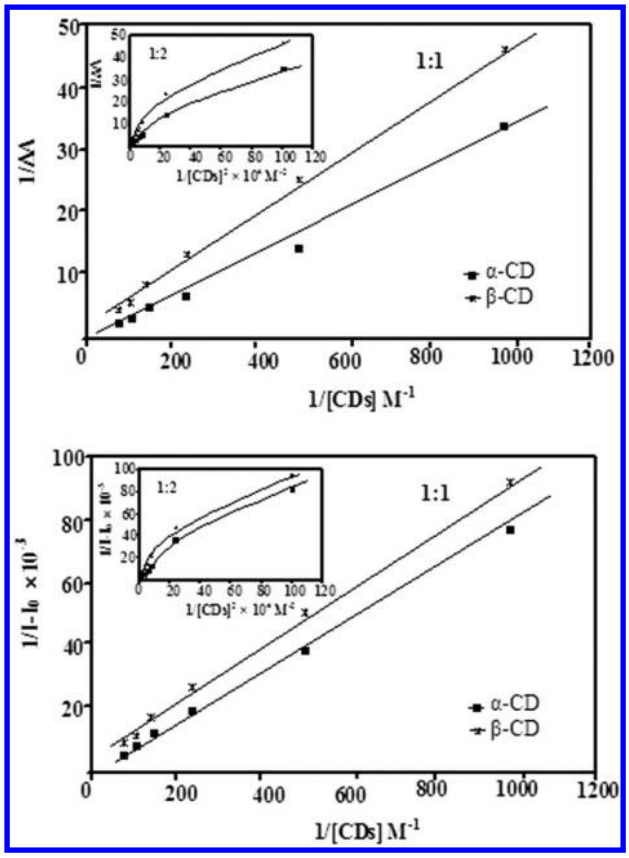

Figure 10. Benesi−Hildebrand plots for the complexation of FBRR with α- and β-CD: (a) $1/\Delta A$ versus $1/[\beta\text{-CD}]$ (inset: $1/\Delta A$ versus $1/[\beta\text{-CD}]^2 \times 10^4\ M^2$) and (b) $1/(I - I_0)$ versus $1/[\beta\text{-CD}]$ {inset: $1/(I - I_0)$ versus $1/[\beta\text{-CD}]^2 \times 10^4\ M^2$}.

emission with increasing β-CD concentration is consistent with this speculation. However, the fact that the ICT emission is greatly enhanced in β-CD solution suggests that rotation of the aniline ring is still feasible in the β-CD cavity. Considering that PICT emission has been observed in solid polymer matrixes and/or under high pressure,[44] it can be concluded that the restriction or increased viscosity in the CD cavity does not affect the formation of the PICT state itself. The enhancement of the PICT emission of β-CD solution should be due to the reduced polarity of the CD environment, as proposed by Nag et al.[40] for DMABN. In a less polar environment, the ICT state is destabilized, and hence, the energy gap between the PICT state and the Franck−Condon (FC) state is increased. This is supported by the blue shift in the PICT emission of FVB upon complexation with β-CD. The increase in the energy gap causes a decrease in the nonradiative transition from the PICT state so that the PICT emission is enhanced. Such an increase in the energy gap is attributable to the reduced dipole−dipole interaction of the PICT state in the CD cavity.

The difference in the binding constants is also responsible for the fact that the I_a/I_b ratio of FBRR/FVB in high-concentration β-CD solution is much higher than that in α-CD solution. In other words, the benzamido ring is more deeply entrapped in the nonpolar β-CD cavity than in the α-CD cavity. Thus, the enhancement of the PICT emission seems to reflect the situation that the aniline ring protrudes in the highly polar aqueous phase where the torsional energy barrier of the amino group for the formation of the PICT state is negligible. Thus, at first glance, the torsional energy barrier for the formation of the

dx.doi.org/10.1021/jp302162g | J. Phys. Chem. B 2012, 116, 9061−9074

Table 3. Binding Energies and HOMO−LUMO[a] Characteristics for the Inclusion Complexes Calculated Using the PM3 Method

property	FBRR	FVB	α-CD	β-CD	FBRR:α-CD	FBRR:β-CD	FVB:α-CD	FVB:β-CD
E_{HOMO} (eV)	−7.99	−7.99	−10.38	−10.35	−8.10	−8.26	−8.09	−8.18
E_{LUMO} (eV)	−0.46	−0.23	1.26	1.23	−0.35	−0.24	−0.18	−0.36
$E_{HOMO} - E_{LUMO}$ (eV)	−7.52	−7.76	−11.64	−11.58	−8.45	−8.01	−7.91	−7.82
μ	−4.22	−4.11	−4.56	−4.56	−4.22	−4.25	−4.14	−4.27
dipole (D)	2.81	3.11	11.34	12.29	11.64	7.15	11.69	12.51
ΔD					−2.51	−7.95	−2.89	−2.76
E (kcal mol^{-1})	−59.82	−31.61	−1247.52	−1457.63	−1316.03	−1528.70	−1285.37	−1498.98
ΔE (kcal mol^{-1})					−8.69	−11.26	−9.74	−6.24
H (kcal mol^{-1})	133.01	157.85	−570.84	−668.16	−444.59	−545.15	−417.58	−518.75
ΔH (kcal mol^{-1})					−6.76	−10.00	−4.59	−8.44
G (kcal mol^{-1})	89.51	113.94	−676.16	−790.14	−577.07	−694.70	−546.74	−666.66
ΔG (kcal mol^{-1})					9.78	5.93	15.68	9.54
S (kcal mol^{-1} K^{-1})	0.145	0.147	0.353	0.409	0.444	0.501	0.433	0.496
ΔS (kcal mol^{-1} K^{-1})					−0.054	−0.053	−0.060	−0.067
zero-point vibrational energy (kcal mol^{-1})	180.28	177.35	634.47	740.56	817.33	921.60	814.28	919.41

[a]HOMO, highest occupied molecular orbital; LUMO, lowest unoccupied molecular orbital.

PICT state is expected to be increased, when considering only the increase of the rise time for the PICT emission. If this were the case, it would result in a marked increase of the normal emission. However, the normal emission was little enhanced compared with the dramatic enhancement of the PICT emission, indicating that the energy barrier was not affected by the entrapment of benzamido ring in the nonpolar β-CD cavity. From this observation, it can be concluded that the energy barrier for the formation of the PICT state is governed not only by the torsion of the amino group but also by the hydrogen bonding between the —CONH— group and water. As long as the hydrogen bonding between the —CONH— group and water is effective, the energy barrier for the PICT does not change. As already discussed, the reverse PICT becomes slower when the —CONH— group is entrapped in the nonpolar β-CD cavity. This should be another reason for the PICT emission to be greatly enhanced in the β-CD complex in contrast to the minimal change in the α-CD complex. In aqueous solution, the back-torsion of the twist conformer formed promptly upon photoinduced charge separation is required for the thermal repopulation of the LE state for the rapid equilibrium between the two emitting species. However, in the restricted environment of the β-CD cavity, the back-torsion of the —CONH— group is inhibited, as demonstrated by observation of the slow rise time in β-CD.

As discussed above, the orientation of FBRR in the β-CD complex is different from that in the α-CD complex, and it is rather similar to that of the FVB/β-CD inclusion complex. As a part of the FBRR molecule is located in the nonpolar α-CD cavity, the PICT emission is expected to be enhanced substantially with an increase in the α-CD concentration, as in the case of the FBRR/β-CD inclusion complex. On the contrary, it was only slightly increased, as shown in Figure 8. From Table 1, it is clear that the relative quantum yield of the slow component of the normal emission was greatly enhanced. Also, the rise time corresponding to the conformational relaxation was too short to be measured even in the high-concentration α-CD solution. In this case, the torsional barrier for the PICT process was negligible, as in the case of the FVB/β-CD inclusion complex.

Nevertheless, the normal emission is rather dramatically enhanced even though the free torsional motion of the —CONH— group is still feasible. Thus, an alternative explanation is possible based on the fact that FBRR has a —CONH— group in contrast to the nitrile group in DEABN as an electron-withdrawing group.[2,3] In aqueous solution, strong hydrogen bonding would be formed between water and the carbonyl group so that the —CONH— group becomes coplanar with the benzene ring. Consequently, this hydrogen bonding seems to make the migration of electron density from benzene to the carbonyl group more facile for the fractional charge separation between benzamido and aniline rings. On the other hand, by entrapment of the carbonyl group in the β-CD cavity, the fractional charge separation is inhibited by the hindrance of hydrogen bonding between water and the carbonyl group. The hindrance of hydrogen bonding is again supported by the decrease in the relative quantum yield of the fast component of normal emission in the β-CD solution (Table 1). Therefore, the normal emission band is enhanced relative to the PICT emission band as the β-CD concentration increases.

3.3. ^{1}H NMR Spectra. To comprehensively examine the structural features of these CD complexes and deeply understand the assembly process, the solution structures of FBRR and FVB were investigated by means of ^{1}H NMR spectroscopy, which showed a certain consistency with the results obtained in the solid state. Generally, the chemical shift values of the guest protons tend to show appreciable changes when the guest molecules are included in the CD cavities.[45,46] Therefore, ^{1}H NMR spectra of FBRR and FVB inclusion complexes were obtained at 25 °C in D_2O and compared with those of FBRR and FVB. The chemical shift values for the FBRR, FVB, and the β-CD inclusion complexes (in parentheses) are as follows. FBRR: NH, 8.30 (8.38); 2′,6′-H, 7.86 (7.93); 3′,4′,5′-H, 7.46 (7.54); 2H, 8.15 (8.13); 5H, 6.36 (6.34); 3OCH_3, 3.81 (3.78); and 6OCH_3, 3.86 (3.85). FVB: NH, 10.40 (10.49); 2′,6′-H, 8.061 (8.10); 3′,5′-H, 7.604 (7.61); 4′-H, 7.695 (7.69); 2H, 8.10 (8.12); 5H, 8.46 (8.45); 3OCH_3, 4.164 (4.162); and 6CH_3, 2.434 (2.433).

As can be seen from these results, the δ value of benzamido protons of FBRR and FVB shifts downfield by up to 0.08 ppm, and the δ values of the aniline ring protons (methoxy and aromatic) shift upfield by up to 0.03 ppm, as compared with the corresponding values for free FBRR and FVB. These results indicate that a host−guest inclusion complex is formed between FBRR or FVB and β-CD in aqueous solution.

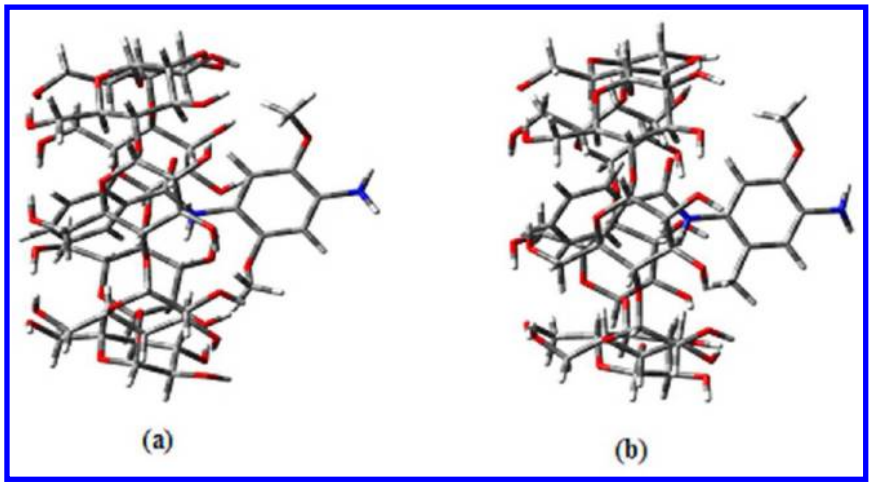

Figure 11. Energy-minimized structures of (a) FBRR:β-CD and (b) FVB:β-CD inclusion complexes at the PM3 level of theory.

3.4. Molecular Modeling. To gain a better understanding of the CD environment, PM3 molecular modeling geometry optimizations were carried out to examine the preferred conformations of the benzamido and aniline moieties in FBRR/FVB. All calculations were performed at the semi-empirical quantum mechanical level of theory with the PM3 method using the program Gaussian 03W. Molecular docking between FBRR, FVB, α-CD, and β-CD was performed by molecular modeling techniques with the aim of constructing reliable models of the complexes. From the crystallographically obtained geometries for the two CDs, [47] geometries were optimized within the force field used. The energies for the calculated minimum conformations were −1247.52, −1457.63, −59.82, and −31.61 kcal/mol for α-CD, β-CD, FBRR, and FVB respectively (Table 3). The symmetry of the CD ring structures was essentially reduced compared to the crystallographic results but was in good agreement with a molecular modeling study on symmetry breaking in cyclodextrins. [48] A detailed analysis of the conformational space of the CDs was performed, calculating 500 low-energy conformers that were generated by statistical variations of geometrical parameters. This study showed that the obtained minima resembled the most prominent low-energy regions.

The distance between the host and guest was defined as the distance between the center of mass of the glycosidic oxygens of CD and the center of mass of the heavy atoms in FBRR or FVB. Optimization was then performed, starting from the minimum CD geometries with the guest positioned at a distance of 10 Å from the center of the CD. The guest molecule was then incrementally pushed through the cavity in 1-Å steps, and the geometry was optimized, starting from the previously minimized structure. This procedure was performed for two sets of reaction coordinates, starting either with the aniline ring or the benzamido moiety pointing toward the CD cavity. For α- and β-CD, this process led to one structure with similar minimum energies, −8.69 and −11.26 kcal/mol for FBRR and −9.74 and −6.24 kcal/mol for FVB, as shown in Figures 1 and 11. It should be pointed out that this procedure gives only one possible reaction coordinate out of a large number, but it resembles all important features of the complex structures.[47,48]

The benzamido moiety is well embedded in the hydrophobic cavity. In the case in which the amino group points toward the primary hydroxylic rim, hydrogen bonding occurs with the glycosidic oxygen; in neither case is the hydroxylic group efficiently shielded from the aqueous environment. In both cases, the long symmetry axes of the aniline moiety of FBRR and FVB are not collinear with the CD axes. The —CONH— system is thus only partly shielded by the hydrophobic cavity; for the lower minimum, the polar group projects freely into the surrounding hydrophilic medium. A small bottleneck was described for inclusion of benzene in α-CD.[47,48]

The formation of the 1:1 guest:host inclusion complexes is clearly anticipated by combining structures in Figure 11. Such structures gain further stabilization energy by hydrogen bonding between hydroxy groups of the primary and secondary rims of the two different CD molecules. Water should be excluded from such a structure, although the small solvent molecules could penetrate the central cavity to interact with the —CONH— or amino group. Similar arguments apply to the 1:1 α-CD complex: The —CONH— and amino groups of FBRR/FVB are well solvated by water molecules, as spectral shifts are even smaller in comparison to those in β-CD. This is supported by the calculated minimum-energy configuration (Figure 11). The large fluorescence intensity observed for the guest:β-CD complex indicates that, in this case, FBRR/FVB forms strong hydrophobic interactions, most likely between an oxygen of the glucosidic link of the CD and —CONH— group of the guest. This is because the electrostatic terms, for example, polar bonds in CD or/and bulk water, add to the red shift. A small Stokes shift (3554 cm^{-1} for FBRR and 4901 cm^{-1} for FVB), similar to that for cyclohexane, indicates only small geometrical rearrangement of the excited-state surface.

3.5. Thermodynamic Parameters. To investigate the thermodynamics of the inclusion process, the binding energies (ΔE), enthalpy changes (ΔH), Gibbs free energy changes (ΔG), and entropy changes (ΔS) for the most stable complexes (α-CD:FBRR, β-CD:FBRR, α-CD:FVB, and β-CD:FVB) were calculated and are summarized in Table 3. The binding energies (ΔE) of the complexes formed by FBRR/FVB passing through the cavities of α-CD and β-CD from the wide side are about 10.0 kJ M^{-1} lower than those formed by approach at the narrow side. Thus, it is predicted that the guest is favored to enter the cavity of CD from its wide side compared to approaching from the narrow side. The standard formation enthalpies (ΔH) of the complexes α-CD:FBRR, β-CD:FBRR, α-CD:FVB, and β-CD:FVB are −6.74, −10.00, −4.59, and −8.44 kcal M^{-1}, respectively, which indicate that the formation reactions for the four complexes are exothermic processes.

dx.doi.org/10.1021/jp302162g | J. Phys. Chem. B 2012, 116, 9061−9074

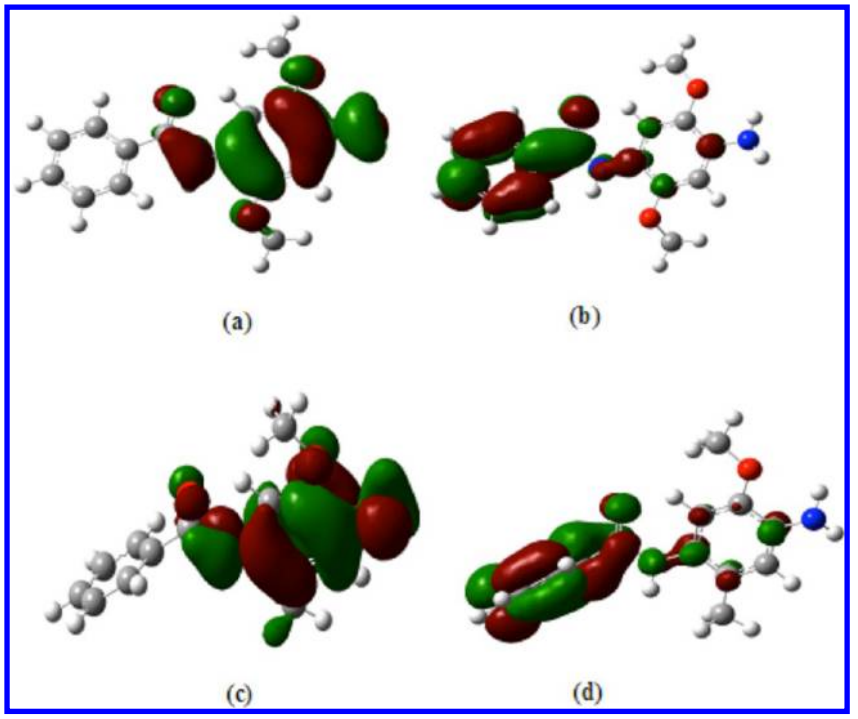

Figure 12. Optimized structures and HOMO−LUMO energy structures of (a) FBRR−HOMO, (b) FBRR−LUMO, (c) FVB−HOMO, and (d) FVB−LUMO.

However, the ΔH values for the α-CD inclusion complexes are lower than those for the β-CD complexes, which indicates that formation of the α-CD complexes is a weak exothermic process. Positive values for the standard Gibbs free energy changes (ΔG) are 9.58, 5.93, 15.68, and 9.54 kcal M^{-1} for the inclusion complexes, α-CD:FBRR, β-CD:FBRR, α-CD:FVB, and β-CD:FVB, respectively. This indicates that the formations of all of the complexes are nonspontaneous processes. The entropy values (ΔS) for the formations of the inclusion complexes are negative (−0.054, −0.053, −0.060, and −0.067 kcal M^{-1} K^{-1} for the inclusion complexes α-CD:FBRR, β-CD:FBRR, α-CD:FVB, and β-CD:FVB, respectively) and make smaller contributions to the positive values of the standard Gibbs free energies than the enthalpy. The negative entropy effect might be due to the combined results of the host−guest reaction (positive contribution to entropy) and releasing of water molecules from the cavity (negative contribution to entropy). Finally, formation of the inclusion complexes α-CD:guest and β-CD:guest are enthalpy−entropy synergistically driven processes.

The positive ΔG values suggest that the formations of all of these inclusion complexes are nonspontaneous processes. However, the experimental data indicate that the formations of all of the inclusion complexes are spontaneous processes. This can be explained by the solvent effect. Unfortunately, because of limitations in the calculation ability of our computer and the large molecular size of cyclodextrins (CDs), calculations for these systems can hardly be performed for aqueous solutions. However, it was observed that the solvent effect on the host−guest interactions easily changes the inclusion reaction from a nonspontaneous process in the gas phase to a spontaneous one in the aqueous phase. The host−guest interaction causes an enthalpy−entropy compensating process in the gas phase, whereas the same interaction causes an enthalpy−entropy codriven process in aqueous solution, because inclusion complexation releases a number of water molecules from the cavity of CDs.

The $(E_{HOMO} - E_{LUMO})$ gap is an important scale of stability,[22] and chemicals with large $(E_{HOMO} - E_{LUMO})$ values tend to have higher stability. Therefore, we investigated the electronic structures of these complexes using the PM3 method. The HOMO and LUMO energies of these guests and their inclusion complexes are shown in Table 3 and Figure 12, which reveal the energy gaps and chemical activities of the molecules. The LUMO as an electron acceptor represents the ability to obtain an electron, and the HOMO represents the ability to donate an electron. Moreover, a lower HOMO−LUMO energy gap explains the eventual stability of a complex; that is, the isolated molecule has a lower stability than complex. Figure 12 illustrates that the HOMO−LUMO energy orbital pictures of these complexes vary significantly. The energy gap between the HOMO and LUMO of each complex suggests that there will be a significant change in the electronic structures of these guest molecules during molecular recognition and binding. The HOMO−LUMO gap for the FBRR:β-CD inclusion complex is most negative, which suggests that this complex is more stable than the other inclusion complexes.

Table 2 presents the interesting bond distances, bond angles, and dihedral angles of the guests before and after complexation in α-CD and β-CD obtained from PM3 calculations from the most stable structure (Figures 1 and 11). It is evident that, in CD, the geometries of the guests were slightly altered. The alterations were significant in dihedral angles, which indicate that the guests adopted specific conformations to form stable complexes. Figure 11 and Table 2 show that the intermolecular hydrogen-bonding distances in the glucosidic bridges are greater than 3.0 Å, which confirms that the guests should not be attached to the oxygens of the glucosidic bridges. Considering the shapes and dimensions of the hosts, the guests might not be completely embedded in the CD cavity.

dx.doi.org/10.1021/jp302162g | J. Phys. Chem. B 2012, 116, 9061−9074

Because the vertical distances and lengths of the guests are greater than the dimensions of the host, the guest molecules cannot be fully present inside the CD cavity. Further, the optimized theoretical structures of the guest:CD inclusion complexes also confirm that the guest molecules are only partially included in the CD cavity.

4. CONCLUSIONS

The following conclusions can be drawn from this study: (i) Dual fluorescence was observed in FBRR and FVB in all of the solvents tested except water. (ii) Similar lifetimes were observed in nonpolar and polar solvents for both states, indicating the presence of equilibrium between them in the S_1 state. (iii) The ratio of the PICT emission to the normal emission of FBRR increased as the β-CD concentration increased, whereas it changed only slightly upon addition of α-CD. (iv) CD dependences of the PICT and normal emission decay of α-CD are quite different from the β-CD. (v) The entrapment of the benzamido ring in the CD cavity seems to inhibit the reverse ICT process by restricted back-torsion from nonplanar to planar conformation of the aniline ring. (vi) ^{1}H NMR spectroscopy indicates that the FBRR/FVB molecules insert their benzamido rings into the cavities of the CDs. (vii) Theoretical studies suggest that hydrophobic interactions play an important role in determining the stability of the inclusion complexes and that the guest is favored to enter the cavities of the CDs from the wide side rather than the narrow side.

AUTHOR INFORMATION

Corresponding Author

*E-mail: drrajendiran@rediffmail.com. Fax: +91 4144 238080. Phone: +91 94866 28800.

Notes

The authors declare no competing financial interest.

ACKNOWLEDGMENTS

This work was supported by the CSIR [No. 01(2549)/12/EMR-II], UGC [No. F-351-98/2011 (SR)] and DST, New Delhi, India (No. SR/FTP/CS-14/2005). A.A.M.P. is thankful to CSIR, New Delhi, India, for the award of a Senior Research fellowship (No. 123029/2K9/1). The authors thank Dr. P. Ramamurthy, Director, and Dr. C. Selvaraju, Assistant Professor, National Centre for Ultrafast Processes, Madras University, for allowing the fluorescence lifetime measurements for this work. We thank Dr. V. K. Subramanian, Department of Chemistry, Annamalai University, for carrying out the grammatical corrections in this article. We also thank the reviewers of this article for their valuable suggestions.

REFERENCES

(1) (a) Lippert, E.; Lüder, W.; Boos, H. In *Advances in Molecular Spectroscopy*; Mangini, A. Ed.; Pergamon Press: Oxford, U.K., 1962; p 443. (b) Lippert, E.; Lüder, W.; Moll, F.; Nägele, H.; Boos, H.; Prigge, H.; Siebold-Blankenstein, I. *Angew. Chem.* **1961**, *73*, 695.

(2) (a) Rettig, W. *Angew. Chem., Int. Ed. Engl.* **1986**, *25*, 971−988. (b) Rettig, W. *J. Lumin.* **1980**, *26*, 21−46. (c) Rettig, W. *Proc. Indian Acad. Sci.* **1992**, *104*, 1−5.

(3) Lippert, E.; Rettig, W.; Bonacic-Koutecky, V.; Heisel, F.; Mieche, J. A. In *Advances in Chemical Physics*; Priogine, I., Rice, S.A., Eds.; Wiley-Interscience: New York, 1987; Vol. *68*, pp 1−173.

(4) (a) Mandal, S.; Rao, V. G.; Ghatak, C.; Pramanik, R.; Sarkar, S.; Sarkar, N. *J. Phys. Chem. B* **2011**, *115*, 12108−12119. (b) Ghosh, A. K.; Samanta, A.; Bandyopadhyay, P. *J. Phys. Chem. B* **2011**, *115*, 11823−11830. (c) Ghosh, A. K.; Samanta, A.; Bandyopadhyay, P. *Chem. Phys. Lett.* **2011**, *507*, 162−167.

(5) (a) Dhenadhayalan, N.; Selvaraju, C.; Ramamurthy, P. *J. Phys. Chem. B* **2011**, *115*, 10892−10902. (b) Sarkar, D.; Ghosh, D.; Das, P.; Chattopadhyay, N. *J. Phys. Chem. B* **2010**, *114*, 12541−12578. (c) Chowdhury, P.; Chakravorti, S. *J. Photochem. Photobiol. A: Chem.* **2006**, *179*, 95−104.

(6) (a) El-Kemary, M.; Organero, J. A.; Santos, L.; Douhal, A. *J. Phys. Chem. B* **2006**, *110*, 14128−14134. (b) Indirapriyadharshini, V. K.; Karunanithi, P.; Ramamurthy, P. *Langmuir* **2001**, *17*, 4056−4060. (c) Arun, K. T.; Jayaram, D. T.; Avirah, R. R.; Ramaiah, D. *J. Phys. Chem. B* **2011**, *115*, 7122−7128.

(7) (a) Tormo, L.; Organero, J. A.; Douhal, A. *J. Phys. Chem. B* **2005**, *109*, 17848−17854. (b) Liu, J. H.; Chiu, Y.-H.; Chiu, T.-H. *Macromolecules* **2009**, *42*, 3715−3720.

(8) (a) Liu, Y.; Chen, Y. *Acc. Chem. Res.* **2006**, *39*, 681−691. (b) Al-Hassan, K. A.; Azumi, T. *Chem. Phys. Lett.* **1988**, *146*, 121−124.

(9) (a) Cho, S. Y.; Allcock, H. R. *Macromolecules* **2009**, *42*, 4484−4490. (b) Terazima, M.; Maeda, K.; Azumi, T.; Tanimoto, Y.; Okada, N.; Itoh, M. *Chem. Phys. Lett.* **1989**, *164*, 562−566.

(10) Grabowski, Z. R.; Rotkiewicz, K.; Siemiarczuk, A.; Cowled, D. J.; Bauman, W. *Nouv. J. Chim.* **1979**, *3*, 443−446.

(11) (a) Khalil, W. S.; Hofeldt, R.; McGlynn, S. P. *Chem. Phys. Lett.* **1975**, *35*, 172. (b) Kosower, E. M.; Dodiuk, H. *J. Am. Chem. Soc.* **1976**, *98*, 924. (c) Visser, R. J.; Varma, C. A. G. O. *J. Chem. Soc., Faraday Trans. 2* **1980**, *76*, 453.

(12) (a) Zachariasse, K. A.; von der Haar, Th.; Hebecker, A.; Leinhos, U.; Kuhnle, W. *Pure Appl. Chem.* **1993**, *65*, 1745. (b) von Der Haar, Th.; Hebecker, A.; Il'Ichev, Y.; Jiang, Y.-B.; Kühnle, W.; Zachariasse, K. A. *Recl. Trav. Chim. Pays-Bas* **1995**, *114*, 430−442.

(13) (a) Zachariasse, K. A.; Grobys, M.; von der Haar, Th.; Hebecker, A.; Il'ichev, Yu. V.; Jiang, Y.-B.; Morawski, O.; Kuhnle, W. *J. Photochem. Photobiol. A: Chem.* **1996**, *102*, 59. (b) Zachariasse, K. A.; Grobys, M.; von der Haar, Th.; Hebecker, A.; Il'ichev, Yu. V.; Morawski, O.; Ruckert, I.; Kuhnle, W. *J. Photochem. Photobiol. A: Chem.* **1997**, *105*, 373.

(14) (a) Il'ichev, Yu. V.; Kuhnle, W.; Zachariasse, K. A. *J. Phys. Chem.* **1998**, *102*, 5670. (b) Zachariasser, K. A. *Chem. Phys. Let.* **2000**, *320*, 8−13.

(15) (a) Prabhu, A. A. M.; Sankaranarayanan, R. K.; Siva, S.; Rajendiran, N. *Spectrochim. Acta A* **2009**, *74*, 484−497. (b) Sivakumar, K.; Stalin, T.; Rajendiran, N. *Spectrochim. Acta A* **2005**, *62*, 991−999.

(16) Antony Muthu Prabhu, A; Sankaranarayanan, R. K.; Siva, S.; Subramanian, V. K.; Rajendiran, N. *Russ. J. Phys. Chem. A* **2010**, *84*, 2270−2283.

(17) (a) Prabhu, A. A. M.; Venkatesh, G.; Rajendiran, N. *J. Solution Chem* **2010**, *39*, 1061−1086. (b) Premakumari, J.; Roy, G. A. G.; Prabhu, A. A. M.; Venkatesh, G.; Rajendiran, N. *J. Phys. Chem. Liq.* **2011**, *49*, 108−132.

(18) (a) Rajendiran, N.; Balasubramanian, T. *Spectrochim. Acta A* **2008**, *69*, 822−829. (b) Stalin, T.; Rajendiran, N. *Spectrochim. Acta A* **2005**, *61*, 3087−3096.

(19) (a) Stalin, T.; Rajendiran, N. *J. Photochem. Photobiol. A: Chem.* **2006**, *182*, 137−150. (b) Stalin, T.; Rajendiran, N. *Chem. Phys.* **2006**, *322*, 311−322. (c) Stalin, T.; Shanthi, B.; Vasantha Rani, P.; Rajendiran, N. *J. Inclusion Phenom. Macrocyclic Chem.* **2006**, *55*, 21−29.

(20) (a) Prabhu, A. A. M.; Venkatesh, G.; Sankaranarayanan, R. K.; Siva, S.; Rajendiran, N. *Indian J. Chem.* **2010**, *49A*, 407−417. (b) Venkatesh, G.; Prabhu, A. A. M.; Rajendiran, N. *J. Fluoresc.* **2011**, *21*, 1485−1497. (c) Prabhu, A. A. M.; Venkatesh, G.; Rajendiran, N. *J. Fluoresc.* **2011**, *20*, 961−972. (d) Premakumari, J.; Roy, G. A. G.; Prabhu, A. A. M.; Venkatesh, G.; Rajendiran, N. *J. Solution Chem.* **2011**, *40*, 327−347.

(21) (a) Meach, S, R. *J. Photochem.* **1983**, *23*, 193. (b) Guilbault, G. G. In *Practical Fluorescence*; Marcel Dekker: New York, 1971; p 13.

(22) (a) Castro, R.; Berardi, M. J.; Cordova, E.; de Olza, M. O.; Kaifer, A. E.; Evanseck, J. D. *J. Am. Chem. Soc.* **1996**, *118*, 10257−10268. (b) Rafati, A. A.; Hashemianzadeh, S. M.; Nojini, Z. B.; Safarpour, M. A. *J. Mol. Liq.* **2007**, *135*, 153−157. (c) Karelson, M.;

Lobanov, V. S.; Katrizky, R. *Chem. Rev.* **1996**, *96*, 1027−1044. (d) Morokuma, K. *Acc. Chem. Res.* **1977**, *10*, 294−300.
(23) Lippert, E. *Z. Naturforsch. A* **1955**, *10*, 541−545.
(24) Reichardt, C.; Dimorth, K. *Fortschr. Chem. Forsch* **1968**, *11*, 1−6.
(25) Kosower, E. M. *An Introduction to Physical Organic Chemistry*; Wiley: New York, 1968.
(26) Beens, H.; Knibbe, H.; Weller, A. *J. Chem. Phys.* **1967**, *47*, 1180−1183.
(27) Khalil, O. S.; Hofeldt, R. H.; McGlynn, S. P. *Chem. Phys. Lett.* **1972**, *19*, 479−482.
(28) (a) Khalil, O. S.; Hofeldt, R. H.; McGlynn, S. P. *J. Lumin.* **1973**, *6*, 229−244. (b) Khalil, O. S.; Meeks, J. L.; McGlyn, S. P. *Chem. Phys. Lett.* **1976**, *39*, 457−461.
(29) (a) Dodiuk, H.; Kosower, E. M. *Chem. Phys. Lett.* **1975**, *34*, 253−257. (b) Kosower, E. M.; Dodiuk, H. *J. Am. Chem. Soc.* **1976**, *98*, 924−929.
(30) (a) Cazeau-Dybroca, C.; Lyazidi, S. A.; Cambou, P.; Peirigua, P.; Cazeau, Ph.; Desquer, M. *J. Phys. Chem.* **1989**, *93*, 2341−2347. (b) Zhang, X.; Sun, X.-Y.; Wang, C.-J.; Jiang, Y.-B. *J. Phys. Chem. A* **2002**, *106*, 5577−5581 and references therein.
(31) Krishnamoorthy, G.; Dogra, S. K. *Chem. Phys.* **1999**, *243*, 45−59.
(32) (a) Mackenzie, R. K.; MacNicol, D. D. *J. Chem. Soc., Chem. Commun.* **1970**, 1299−1303. (b) Brand, C. D.; Williams, D. R.; Cook, T. J. *J. Mol. Spectrosc.* **1966**, *20*, 359−380.
(33) Rettig, W.; Vogel, M.; Lippert, E.; Otto, H. *Chem. Phys.* **1986**, *103*, 381−384.
(34) Changenet, P.; Plaza, P.; Martin, M. M.; Meyer, Y. H. *J. Phys. Chem.* **1997**, *101*, 8164−8168.
(35) (a) Guillaume, B. C. R.; Yogev, D.; Fendler, J. H. *J. Phys. Chem.* **1991**, *95*, 7489−7494. (b) Nag, A.; Dutta, R.; Chattopadhyay, N.; Bhattacharyya, K. *Chem. Phys. Lett.* **1989**, *157*, 83−86.
(36) Kajimoto, O.; Nayuki, T.; Kobayashi, T. *Chem. Phys. Lett.* **1993**, *209*, 357−360.
(37) Kim, Y. H.; Cho, D. W.; Yoon, M.; Kim, D. *J. Phys. Chem.* **1996**, *100*, 15670−15676.
(38) (a) Jiang, Y. B. *Appl. Spectrosc.* **1994**, *48*, 1169−1173. (b) Jiang, Y. B. *J. Photochem. Photobiol. A: Chem.* **1995**, *88*, 109−116.
(39) (a) Cho, D. W.; Kim, Y. H.; Kang, S. G.; Yoon, M.; Kim, D. *J. Phys. Chem.* **1994**, *98*, 558−562. (b) Cho, D. W.; Kim, Y.; Kang, S. G.; Yoon, M.; Kim, D. *J. Chem. Soc., Faraday Trans.* **1996**, *92*, 29−33.
(40) (a) Nag, A.; Dutta, R.; Chattopadhyay, N.; Bhattacharyya, K. *Chem. Phys. Lett.* **1989**, *157*, 83−86. (b) Nag, A.; Bhattacharyya, K. *Chem. Phys. Lett.* **1988**, *151*, 474−476.
(41) (a) Wang, Y.; Eisenthal, K. B. *J. Chem. Phys.* **1982**, *77*, 6076−6082. (b) Kundu, S.; Chattopadhyay, N. *J. Photochem. Photobiol. A: Chem.* **1995**, *88*, 105−108. (c) Al-Hassan, K. A.; Klein, U. K. A.; Suwaiyan, S. *Chem. Phys. Lett.* **1993**, *212*, 581−587.
(42) Szejtli, J. *Cyclodextrin Technology*; Kluwer Academic Publishers: Dordrecht, The Netherlands, 1988; pp 143−154.
(43) Benesi, H. A.; Hildebrand, J. H. *J. Am. Chem. Soc.* **1949**, *71*, 2703−2707.
(44) Cazeau-Dubroca, C.; Peirigua, A.; Lyazidi, S. A.; Nouchi, G.; Cazeau, Ph.; Lapouyade, R. *Chem. Phys. Lett.* **1986**, *124*, 110−115.
(45) (a) Sainz-Rozas, P. R.; Isasi, J. R.; Sanchez, M.; Tardajos, G.; Gonzalez-Gaitany, G. *J. Phys. Chem. A* **2004**, *108*, 392−402. (b) Rath, M C.; Palit, D. K.; Mukherjee, T. *J. Chem. Soc., Faraday Trans.* **1998**, *94*, 1189−1196.
(46) Nakashima, H.; Takenaka, Y.; Higash, M.; Yoshida, N. *J. Chem. Soc., Perkin Trans. 2* **2001**, 2096−2103.
(47) (a) Chako, K. K.; Saenger, W. *J. Am. Chem. Soc.* **1981**, *103*, 1708−1715. (b) Betzel, C.; Saenger, W. *J. Am. Chem. Soc.* **1984**, *106*, 7545−7557.
(48) (a) Park, H. R.; Mayer, B.; Wolschann, P.; Kohler, G. *J. Phys. Chem.* **1994**, *98*, 6158−6166. (b) Lipkowitz, K. B.; Raghotama, S.; Yang, J. A. *J. Am. Chem. Soc.* **1992**, *114*, 1554−1562.